Electrical Power and Energy Systems 175 (2026) 111645

Contents lists available at ScienceDirect

International Journal of Electrical Power and Energy Systems

journal homepage: www.elsevier.com/locate/ijepes

Decentralised consensus-based hierarchical control of a hybrid AC–DC microgrid robust to communication delays

Andrés Tomás-Martín [a,*], Behzad Kazemtabrizi [b], Aurelio García-Cerrada [a], Lukas Sigrist [a], Emilio J. Bueno [c]

[a] IIT, ETSI ICAI, Comillas Pontifical University, calle Alberto Aguilera, 23, 28015, Madrid, Spain
[b] Department of Engineering, Durham University, South Road, DH1 3LE, Durham, United Kingdom
[c] Department of Electronics, University of Alcalá, 28805, Alcalá de Henares, Spain

ARTICLE INFO

Keywords:
Consensus
Decentralised control
Economic dispatch
Hierarchical control
Microgrids

ABSTRACT

The continuous growth of distributed renewable energy resources in medium and low-voltage networks supports the case for a distributed architecture for electricity supply relying on microgrids. Whereas decentralised architectures for the primary and secondary control layers of the hierarchical control of microgrids have already been proposed, the tertiary control (economic dispatch) has been mainly formulated as a centralised control or as a distributed control that relies on a central agent to coordinate the operation between distributed generators. This paper proposes a fully decentralised hierarchical microgrid control based on a consensus-based economic dispatch problem. Unlike the proposals found in the literature, the convergence of the proposed tertiary control layer is robust to communication delays and the secondary control layer applies an incremental formulation for a seamless integration with the tertiary layer. The robustness and performance of the proposed hierarchical control are compared with those of a conventional centralised approach and a previously published decentralised approach. The proposal is validated using detailed non-linear real-time simulations, and its stability is proved by modal analysis and using Lyapunov functions.

1. Introduction

1.1. Context

Generation at the distribution level is gradually increasing in modern power systems, led by the penetration of renewable energy sources. Currently, most generation resources at the distribution level are connected to the power system by means of electronic power converters which are able to provide unprecedented flexibility. This scenario calls for new proposals for the way in which power systems are operated. For example, the concept of microgrid [1] has arisen as a proposal for the modernisation of the power sector. A microgrid is understood as an autonomous electric system with generation, loads, and control capable of operating in islanded or grid-tied mode.

Like in conventional power systems, microgrids are usually controlled hierarchically with three layers, with several applications of hierarchical control for DC microgrids [2] and AC microgrids [3,4]. In the case of AC microgrids:

- The primary control is in charge of stabilising the voltage and frequency of the microgrid. It is typically a purely local control, relying on local measurements only [3].
- The secondary control is in charge of recovering the voltage and frequency (and optionally the power interchange) to their nominal values after the action of the primary control.
- The tertiary control is in charge of the optimal operation of the microgrid (e.g., the economic dispatch of generators within the microgrid). This layer also controls the power flow between the microgrid and the main grid in grid-tied operating mode.

Secondary and tertiary control can be carried out in a centralised manner (i.e. measurements are collected in a central controller where control actions are decided) such as in automatic generation control or the voltage control based on pilot buses [5], but they can also be carried out using distributed or decentralised strategies as in [6–8], where the definitions of distributed and decentralised control are not unique. In this paper, a "distributed control" refers to a control where agents use local measurements, information from neighbours, and information from a central coordinator, whereas a "decentralised control" denotes a control where agents only use local measurements and information from neighbours (see [7,8]).

* Corresponding author.
E-mail address: atomas@comillas.edu (A. Tomás-Martín).

https://doi.org/10.1016/j.ijepes.2026.111645
Received 21 July 2025; Received in revised form 17 November 2025; Accepted 24 January 2026
Available online 2 February 2026

List of main symbols

Sets and Indexes

U	Set of generating units in a general case.
N	Set of vertices in a graph. Set of agents in a multi-agent control problem.

Parameters

c_{A_i}	Quadratic cost coefficient of agent i [\$/MW^2].
c_{B_i}	Linear cost coefficient of agent i [\$/MW].
c_{C_i}	Constant cost coefficient of agent i [\$].
γ_i	Gain of agent i for the convergence of the virtual marginal cost consensus.
a_{ij}^{Ter}	ith-row and jth-column element of the adjacency matrix for the economic dispatch.
a_{ij}^{ω}	ith-row and jth-column element of the adjacency matrix for the frequency consensus.
a_{ij}^{P}	ith-row and jth-column element of the adjacency matrix for the active-power consensus.
a_{ij}^{v}	ith-row and jth-column element of the adjacency matrix for the voltage consensus.
a_{ij}^{Q}	ith-row and jth-column element of the adjacency matrix for the reactive-power consensus.

Variables

$\lambda_{v,i}$	Virtual marginal cost of agent i [\$/MW].
P_i^*	Active-power set point of agent i obtained by the economic dispatch algorithm [MW].

A common approach for decentralised control is what is known as "consensus" [9], where agents (e.g., generating unit) work cooperatively based on the communication among neighbouring agents. This paper proposes a fully decentralised hierarchical control for microgrids, based on two novel consensus-based algorithms for the tertiary and secondary control layers and using local droop-based primary controls.

1.2. Literature review

Tertiary control is responsible for generating set points for the secondary control layer by planning the use of the different active- and reactive-power resources available. It commonly assumes steady-state operation of the power system. According to the time horizon of the tertiary control, it spans from generation resource scheduling (e.g., unit commitment [10]) to economic dispatch [11,12] and optimal power flow problems [13], commonly used for near-real-time operational optimisation [14].

The economic dispatch is a particular case of the optimal power flow by either partially (e.g., by considering active-power flows only) or fully neglecting the grid [15] and both centralised and distributed algorithms have been proposed.

Centralised algorithms determine the active power set points by essentially solving an optimisation problem subject to element and system-related constraints. The optimisation problem can be extended to include uncertainties [12] and security constraints [16]. Following the trend of decentralising control and decision taking, distributed control algorithms have also been applied to solve the economic dispatch, although a central coordinator agent is still needed. For example, consensus-based control [15,17] or game theory [18] have been proposed. The central coordinator in the distributed economic dispatch problem is usually one agent guaranteeing the generation-demand balance with a global vision [19]. A distributed consensus-based economic dispatch for multi-microgrids is proposed in [20], with each microgrid solving a centralised economic dispatch problem. Although the economic dispatch problem is usually addressed without considering grid constraints and losses, some distributed algorithms do consider losses [21]. The designed grid capacity of microgrids is typically sufficient to handle power flows without congestion. In fact, many markets (at least in Europe) are cleared without grid constraints, which are checked in a subsequent step; and in microgrids, although the voltage profile is important, this constraint is not normally considered in the economic dispatch problem [17].

A fully decentralised consensus-based formulation for the economic dispatch problem is proposed in [22]. This algorithm is generalised for a directed graph in [23], guaranteeing the demand-generation balance by communicating each agent's demand-generation imbalance to their neighbours and introducing a learning gain. An analysis of how communication delays impact the performance of the algorithm proposed in [23] is presented in [24] and finds limits for its convergence based on the maximum expected delay. Recently, new developments on decentralised economic dispatch have addressed stochasticity using approximate dynamic programming [25], the consideration of ramp constraints [26], and the introduction of line losses [27].

Secondary control is responsible for generating set points for the primary control layer. Consensus has been widely applied to secondary control. Consensus formulation is applied to the adaptive droop control of a DC microgrid in [28] to balance the state of charge of the batteries within a microgrid and carry out voltage regulation. In AC systems, consensus readily works for controlling frequency and sharing active power among generation units after a disturbance in microgrids with inductive lines, whereas a compromise must be reached between reactive-power sharing and bus voltage control since reactive-power flow depends on the voltage profile [29]. In this regard, [30] gives different weights to voltage control and reactive power control. Power-sharing is commonly achieved by either imposing the global active-power sharing of distributed generators (DGs) according to the rated power of the units [4,31] or by taking into account generation costs of each unit in the dynamic control of the system [32]. The latter makes the tertiary control layer vulnerable to communication time delays since it is included in the real-time control.

Communications in consensus-based secondary control can be done continuously or in an event-triggered manner. In the former, messages are sent as soon as the communication channel is available. This keeps the communication channel used all the time and eases the modelling, analysis, design and implementation of the secondary control layer. In the latter, messages are sent only when the change in the value of the variable to be sent with respect to the previous message is above a threshold [6,33]. This threshold can be constant [34] or variable [35]. An event-triggered secondary control is used for the adaptive droop control of a DC microgrid in [36] to reduce the number of messages sent. Although an event-triggered secondary control reduces the communication channel usage, it requires careful design of the trigger mechanism, and it complicates the detection of the loss of agents and the stability analysis of the system. This technique has also been applied to the online optimisation of the operation of a power system in [37] with the same objective of reducing the number of messages sent.

For continuous communication, Ref. [38] shows that the stability of consensus-based secondary control is strongly affected by communication delays and it demonstrates that, for a given communication graph, the attainable consensus convergence speed is limited by a maximum allowable communication delay.

The robustness of the secondary control to communication delays can be improved by adding extra feedback signals [39], or by using a delay compensation method [40,41].

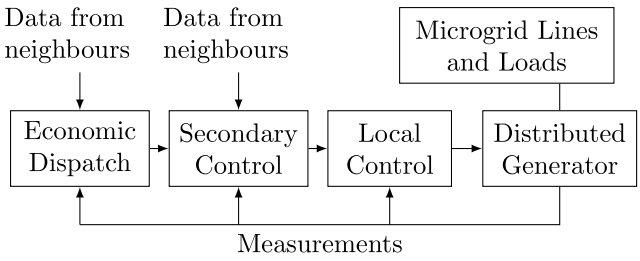

Fig. 1. Overview of the proposed decentralised hierarchical control for a microgrid, implemented for each generator of the microgrid.

1.3. Overview of the system model and the proposed control

This section describes the characteristics of the fully decentralised hierarchical control proposed for a hybrid DC/AC microgrid.

Fig. 1 shows a general overview of the proposed hierarchical control applied to one generator of the microgrid. The structure of the tertiary and secondary control layers is the same for each agent (generator) of the microgrid, and there is no need for central coordination. The primary control is implemented locally, and the secondary and tertiary control layers only require communication between some generators, called neighbours.

The tertiary control solves the economic dispatch problem by means of a consensus algorithm and sends the computed set points to the secondary control. Since previously proposed decentralised tertiary controls present limited convergence in the case of communication delays and were found to require a specific graph property (the adjacency matrix must be doubly stochastic [25]); an event-triggered strategy is proposed here to achieve robustness to communication delays. The tertiary control is run every n seconds and relies on the inner control layers to meet the required set points before the next update. In this paper, the performance of the proposed tertiary control is compared to existing centralised and decentralised approaches to provide a comprehensive overview. Unlike in most references in the literature, the evaluation of the tertiary control performance is carried out using a detailed simulation of the inner control layers.

The proposed secondary control also makes use of a consensus algorithm based on continuous communication. Contrary to existing approaches, the secondary control uses an incremental formulation, acting on deviations of the set points issued by the tertiary control. It is designed to handle the demand variations by considering the units' costs (i.e., the active-power sharing, among units, of a disturbance is inversely proportional to their costs). This novel incremental formulation was inspired by traditional centralised incremental secondary control (e.g., automatic generation control [42]), and achieves the required active- and reactive-power sharing of the deviations from the set-points scheduled by the tertiary control layer, considering active-power limits of generation units. In this paper, its performance is compared to a more conventional consensus approach in which changes in demand are initially shared by generation units according to their rated power [9]. Finally, the robustness of the proposed incremental secondary control algorithm to communication delays is assessed by using modal analysis. The proposed incremental secondary control can be readily extended to include event-triggered communications, extra feedback signals or delay compensation methods to increase its robustness to communication delays. Meanwhile, the voltage control implemented in this paper is limited to reactive-power sharing in the secondary control layer and voltage/reactive-power droop in the primary control layer, as it is commonly presented for microgrids [9]. Nevertheless, advanced voltage control techniques, like those proposed in [21] and [30], could also be applied with the proposed incremental formulation.

1.4. Summary of the paper contributions

The contributions of this paper can be summarised as follows:

- A fully decentralised hierarchical control for microgrids is proposed, and its performance is validated with a detailed simulation of all control layers. The main results of the decentralised hierarchical control are analysed in detail and validated by real-time simulations of a non-linear dynamic model of an AC/DC hybrid microgrid.
- A novel decentralised tertiary control is presented that converges regardless of the communication time delay between agents and does not need a central coordination agent.
- A novel incremental decentralised secondary control is presented and validated. It considers the active power limits of the distributed generators and is able to account for unit costs.

Table 1 compares the main contributions of the proposed hierarchical control structure to some existing approaches.

2. Decentralised economic dispatch problem

The tertiary control layer is responsible for the optimal operation of the microgrid and the control of the power exchange between the microgrid and the main grid. The tertiary control layer is dynamically decoupled from the primary and secondary control layers. In fact, the timescales for different functionalities of the tertiary control layer can differ significantly. Timescales can go from a few seconds (for example, an online optimal power flow calculation) to minutes or hours (for example, the economic dispatch problem) or even days (for example, the unit commitment problem). For the tertiary control layer, this paper implements a decentralised version of the economic dispatch problem.

2.1. Centralised economic dispatch problem

The traditional economic dispatch problem for a set U of generation units without considering grid constraints is commonly formulated as [43]:

$$\begin{cases} \min & \sum_{i\in U} C_i \\ \text{with} & C_i = c_{A_i} P_i^2 + c_{B_i} P_i + c_{C_i} \\ s.t. & \sum_{i\in U} P_i = P_L \\ & P_{i,\min} \le P_i \le P_{i,\max} \quad \forall\, i \in U \end{cases} \tag{1}$$

where P_i is the active power supplied by the ith generation unit, C_i is the unit's cost to produce P_i, c_{A_i}, c_{B_i} and c_{C_i} are its cost coefficients, $P_{i,min}$ and $P_{i,max}$ are its minimum and maximum generating limits, respectively, and P_L is the total load.

If generator power limits are not reached (i.e., $P_{i,\min} < P_i < P_{i,\max}$, $\forall i$), the unconstrained problem can be formulated using the following Lagrangian function:

$$L\left(P_{i\in U}\right) = \sum_{i\in U} C_i\left(P_i\right) + \lambda\left(P_L - \sum_{i\in U} P_i\right) \tag{2}$$

where λ is the Lagrange multiplier, which can be calculated using the optimality conditions (Karush–Kuhn–Tucker (KKT) conditions) [44]:

$$\frac{\partial L}{\partial \lambda} = 0 \tag{3}$$

$$\lambda = \frac{\partial C_i}{\partial P_i} = 2c_{A_i} P_i + c_{B_i},\ \forall i \tag{4}$$

The Lagrange multiplier is the dual variable or shadow price, representing the change in the value of the objective function when there is a unit change in demand. In marginal pricing approaches, there is a single price for the system.

Table 1
Summary of the main contributions of the proposed hierarchical control structure compared to some existing approaches.

Reference	Structure	TC	TC delay robust.	SC formulation
[4]	Centralised	✓		Incremental
[20]	Distributed	✓		
[9]	Decentralised			Absolute
[32]	Decentralised	✓	Limited	TC integrated into SC
[23]	Decentralised	✓		
[24]	Decentralised	✓	Limited	
[30]	Decentralised	✓	Limited	Voltage control in TC
This paper	Decentralised	✓	Fully (Triggered)	Incremental

TC: Tertiary control, SC: Secondary control.

If any of the power generation constraints of a generation unit $i \in U$ is reached:

$$\begin{cases} 2c_{A_i}P_i + c_{B_i} < \lambda, & \text{for } P_i = P_{i\,\max} \\ 2c_{A_i}P_i + c_{B_i} > \lambda, & \text{for } P_i = P_{i,\min} \end{cases} \tag{5}$$

2.2. The economic dispatch as a consensus problem

In a decentralised control approach, each generation unit is an agent that will make decisions based on local measurements and limited information from neighbours. Usually, the communication structure among agents is formulated with the help of a graph $G = (N, E)$ consisting of n vertices (or nodes) $N = \{v_i | i = 1, 2, \dots, n\}$, and a set of edges that connect pairs of nodes $E \subseteq N \times N$. Agents are placed at nodes and edges represent the communication links between agents [45]. Directed graphs (digraphs) have a direction associated with each edge. In this case, an edge is typically represented as a pair $\{v_i, v_j\}$, which means that the information goes from agent v_i to agent v_j. An n-node graph has an $n \times n$ adjacency matrix $\mathbf{A}_G$ which has the weights for the communication links:

$$\begin{cases} a_{ij} > 0 & \{v_j, v_i\} \in E \\ a_{ij} = 0 & \{v_j, v_i\} \notin E \end{cases} \tag{6}$$

In a digraph, if $a_{ij} > 0$ node v_i receives information from its neighbour node v_j but not necessarily vice versa. The set of neighbours of node v_j is defined as $N_j = \{v_i | \{v_i, v_j\} \in E\}$.

2.3. Consensus in multi-agent control systems with a leader node

Following the approach in [46], let us assume that the state of nodes v_i and v_j can be quantified as $x_i(t)$ and $x_j(t)$, respectively, at a given time instant t. Let us also assume that v_i controls its state value as:

$$\frac{dx_i(t)}{dt} = \sum_{v_j \in N} a_{ij}\left[x_j(t) - x_i(t)\right] + b_i\left[x_{ref} - x_i(t)\right] \tag{7}$$

where $b_i \geq 0$ for only one node called "the leader" with a state value of x_{ref}.

Consensus is reached if

$$\lim_{t\to\infty} \frac{dx_i(t)}{dt} = 0 \tag{8}$$

and

$$\lim_{t\to\infty} x_1(t) = \cdots = \lim_{t\to\infty} x_n(t) = x_{ref} \tag{9}$$

which are guaranteed if and only if the leader node is the root of a spanning tree in the graph, i.e., all nodes of the graph can be reached from the leader by following the directed edges of the graph. This condition can be verified by evaluating the eigenvalues of the Laplacian matrix of the graph, a matrix constructed from the adjacency matrix. More details on consensus algorithms and their stability can be found in [46].

As shown in the previous section, the optimality conditions are met when $2c_{A_i}P_i + c_{B_i}$ of all non-limited units are equal (λ). Therefore, one could formulate the economic dispatch as a fully decentralised problem implementing consensus on the marginal costs that will be assumed to have different values in each unit ($\lambda_{v,i} \neq \lambda_{v,j}$):

$$\frac{dP_i^*(t)}{dt} = \gamma_i \overbrace{\sum_{j\in N} a_{ij}^{Ter}\left(\lambda_{v,j}(t) - \lambda_{v,i}(t)\right)}^{\text{consensus on virtual marginal cost}} \tag{10}$$

with $P_i^*(t=0) = P_i$ at the instant of running the economic dispatch problem, γ_i is a dimensionless gain that can be tuned to adapt the speed of convergence (its design is shown later), and:

$$\lambda_{v,i}(t) = \frac{\sum_{j\in N} a_{ij}^{Ter}\lambda_{v,j}(t-\sigma)}{\sum_{j\in N} a_{ij}^{Ter}}, \quad \begin{cases} \text{if } P_i^*(t) = P_{i,\min} \text{ or} \\ \text{if } P_i^*(t) = P_{i,\max} \end{cases} \tag{11}$$

$$\lambda_{v,i}(t) = 2c_{A_i}P_i + c_{B_i} \text{ if } P_{i,\min} < P_i^*(t) < P_{i,\max} \tag{12}$$

where $0 < \sigma << 1$.

To guarantee that the power generation in each unit is within constraints, $P_i^*(t)$ is limited to the range $[P_{i,\min}, P_{i,\max}]$. If $P_i^*(t)$ reaches saturation, $\lambda_{v,i}(t)$ can be obtained from the ones calculated by the neighbours, as in (11).

The proof of convergence of the proposed decentralised algorithm to solve the economic dispatch problem is included in Appendix A.

2.3.1. Demand constraint requirement

The demand constraint requirement in the economic dispatch problem is:

$$\sum_{i\in U} P_i = P_L \tag{13}$$

where P_i is the active power supplied by the ith generator and P_L is the total demand (or load).

In the centralised problem, the total demand P_L is estimated as the sum of the active power served by the generators at the operating point:

$$P_L = \sum_{i\in N} P_i(0) \tag{14}$$

This is achieved if the total generation power remains constant:

$$\sum_{i\in N} \frac{dP_i^*(t)}{dt} = 0 \tag{15}$$

Therefore, the demand constraint is satisfied as long as the saturated units act as pass-through agents, which is ensured by Eq. (11).

2.3.2. Introducing generation limits for agents

Unlike in most cases [47], the convergence of the proposed algorithm does not change under saturations. A demonstration follows.

When applying the general consensus algorithm, units limit their active power set point in the range $[P_{min}, P_{max}]$. During this saturation, the virtual marginal cost changes as:

$\lambda_{v,i}(t) =$

$$\begin{cases} \dfrac{\sum_{j\in N} a_{ij}^{Ter}\lambda_{v,j}(t)}{\sum_{j\in N} a_{ij}^{Ter}} & \text{for } P_i^*(t) = P_{i,\min} \\ \dfrac{\sum_{j\in N} a_{ij}^{Ter}\lambda_{v,j}(t)}{\sum_{j\in N} a_{ij}^{Ter}} & \text{for } P_i^*(t) = P_{i,\max} \\ 2c_{A_i}P_i + c_{B_i} & \text{for } P_{i,\min} < P_i^*(t) < P_{i,\max} \end{cases} \tag{16}$$

From a practical point of view, this is a feedforward of the values received by the neighbours during saturation. This guarantees the consensus between all non-saturated agents that remain communicating their own values.

2.3.3. Convergence under time delays

Communication time delays among agents can affect the convergence of the consensus algorithm [24,48]. If τ_{ji} were the communication delay between unit j and unit i, (10) should be written as:

$$\frac{dP_i^*(t)}{dt} = \gamma_i \overbrace{\sum_{j\in N} a_{ij}^{Ter}\left(\lambda_{v,j}(t-\tau_{ji}) - \lambda_{v,i}(t)\right)}^{\text{consensus on virtual marginal cost}} \tag{17}$$

Here, the delay bound to guarantee the stability of the consensus algorithm is limited by the maximum out-degree (i.e., $\max_j(\sum_i \gamma_i a_{ij})$) of the nodes of the graph, affected by both a_{ij} and γ_i, as stated by [38].

2.3.4. Discrete-time implementation

A new discrete implementation of the problem is introduced here to avoid problems with delays (making the economic dispatch convergence independent from the communication delay between agents): each iteration is only run at each agent when all the messages from its neighbours are received, guaranteeing robustness to communication delays and to asynchronous communications. This discrete implementation will be called "triggered".

$$P_i^*(k+1) = P_i^*(k) + \gamma_i \overbrace{\sum_{j\in N} a_{ij}^{Ter}\left(\lambda_{v,j}(k) - \lambda_{v,i}(k)\right)}^{\text{consensus on cost}} \tag{18}$$

2.3.5. Calculation of the convergence gain

To calculate the convergence gain γ_i to be used in (18) in the discrete system, we have to consider the power limits. Considering that, in a discrete system, the consensus is only guaranteed if the states cannot pass from the minimum limit to the maximum limit or vice versa in only one iteration [47], Eq. (18) can be rewritten as:

$$P_i^*(k+1) = P_i^*(k) + \Gamma_i \tag{19}$$

where the bounds of Γ_i that guarantee consensus in the discrete system are:

$$\begin{cases} \max(\Gamma_i) < P_{i,max} - P_{i,min} \\ \min(\Gamma_i) > P_{i,min} - P_{i,max} \end{cases} \tag{20}$$

If for simplicity, $\gamma = \gamma_i = \gamma_j \ \forall\, i,j$, and taking into account (18) and (20), one obtains:

$$\gamma < \frac{\min_i\left(\dfrac{P_{i,max} - P_{i,min}}{c_{B_i} + c_{A_i}P_{i,max}^2}\right)}{\max_i\left(\sum_j a_{ij}\right)} \tag{21}$$

3. Decentralised increment-based secondary control

This paper proposes an increment-based secondary control layer also based on consensus which acts only on deviations from the tertiary control set points. Generation or demand variations from the dispatched values and power losses cause these deviations. The incremental notation used for secondary control is described by Eqs. (22)–(25):

$$\frac{d\Delta\omega_i^{ref}}{dt} = \sum_{j\in N} a_{ij}^{\omega}(\Delta\omega_j^{ref} - \Delta\omega_i^{ref}) - g_i^{\omega}\Delta\omega_i^{ref} \tag{22}$$

$$\frac{d\Delta P_i^{ref}}{dt} = \sum_{j\in N} a_{ij}^{P}\left(\frac{\Delta\omega_j - \Delta\omega_i}{m_{P_i}} + \Delta P_j - \Delta P_i\right) - g_i^{P}\Delta P_i - g_i^{\omega}\Delta\omega_i \tag{23}$$

$$\frac{d\Delta v_i^{ref}}{dt} = \sum_{j\in N} a_{ij}^{v}(\Delta v_j - \Delta v_i) - g_i^{v}\Delta v_i \tag{24}$$

$$\frac{d\Delta Q_i^{ref}}{dt} = \sum_{j\in N} a_{ij}^{Q}(\Delta Q_j - \Delta Q_i) - g_i^{Q}\Delta Q_i \tag{25}$$

where, with x being the frequency (ω), active power (P), reactive power (Q), or voltage (V), Δx_i^{ref} is the increment from the reference value given by the tertiary control ($x_i^{ref,T}$), i.e., $\Delta x_i = x_i - x_i^{ref,T}$ is the measured deviation from the tertiary control reference, g_i^x are the pinning gains for frequency, active and reactive power. Meanwhile, a_{ij}^x are the elements of the adjacency matrices for frequency, active and reactive power, and voltage.

The proof of convergence of the proposed incremental secondary control is included in Appendix B.

This paper adopts the leader-based pinning gain procedure used by [9], in which only the DGs set as the leaders could have non-zero pinning gains and, for simplicity, only one leader will be considered in the system. It is in charge of recovering the voltage and frequency of the system after any disturbance. Therefore, if the leader is the DG k:

$$g_k^{\omega} = g_k^{v} = 1 \quad \& \quad g_i^{\omega} = g_i^{v} = 0 \ \ \forall\, i \neq k \tag{26}$$

The proposed method does not involve pinning gains for active and reactive power:

$$g_i^{P} = g_i^{Q} = 0 \ \ \forall\, i \tag{27}$$

As mentioned by [29], in power systems with highly inductive electrical lines, voltage and reactive power are strongly coupled. Given the fact that the voltage is a local variable for each agent, as opposed to the frequency, consensus on a voltage profile and reactive power distribution cannot be achieved simultaneously. This means that in (24) and (25), $\forall\ i,j$, if $a_{ij}^{v} = 1$ then $a_{ij}^{Q} = 0$ and if $a_{ij}^{Q} = 1$ then $a_{ij}^{v} = 0$. This application prioritises reactive power consensus in the secondary control layer over voltage consensus.

The active power set points calculated by the secondary control are saturated to consider the DGs operating range. If the leader were with its active power set point saturated, its role would be passed to the next DG that is not saturated, because some active power margin is necessary to recover the system frequency.

3.1. Cost-based secondary control

To consider unit costs in the secondary control layer, a_{ij}^{P} coefficients can be modified as:

$$a_{ij}^{P,cost} = a_{ij}^{P}\frac{dc_j}{dc_i\sum_j \dfrac{dc_j}{dc_i'}} \tag{28}$$

where:

$$dc_i = \frac{\partial c_i}{\partial P_i} = 2c_{A_i}P_i + c_{B_i} \tag{29}$$

If the measured active power of the units is above their scheduled active power, the most expensive must have the lowest increment. If the measured active power of the units is below their scheduled active power, the most expensive must have the highest decrement. To change the active-power sharing if the scheduled active power is above the measured one, a_{ij}^{P} can be modified further as:

$$dc_i = \begin{cases} \dfrac{\partial c_i}{\partial P_i} = 2c_{A_i}P_i + c_{B_i} & \Delta P_i > 0 \\ \left(\dfrac{\partial c_i}{\partial P_i}\right)^{-1} = \dfrac{1}{2c_{A_i}P_i + c_{B_i}} & \Delta P_i < 0 \end{cases} \tag{30}$$

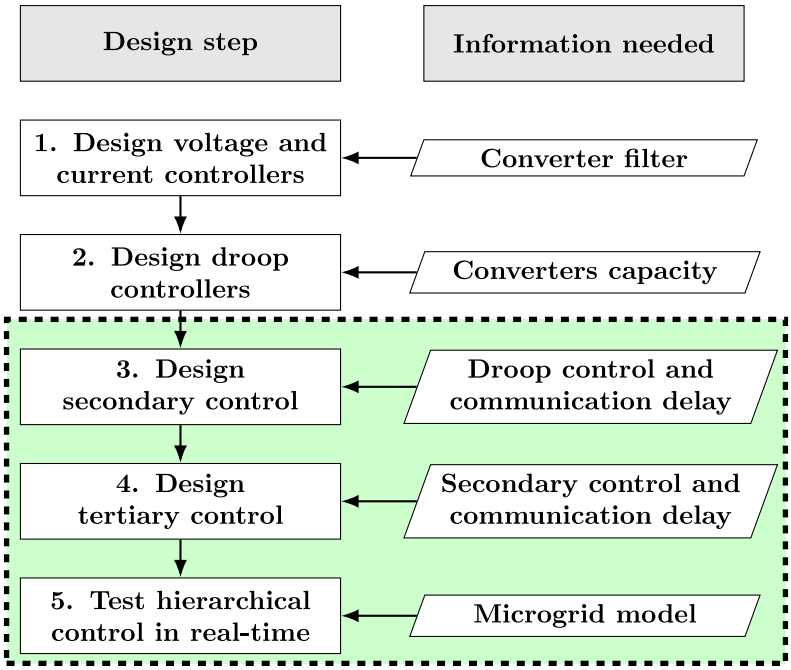

Fig. 2. Flowchart of the design of the proposed decentralised hierarchical control structure, specified for grid-forming converters. The dashed area includes the control layers with novelties described in this paper.

Generation units have two main control solutions: Grid-forming (imposing voltage and frequency at their connection point) and grid-following (tracking voltage and frequency at their connection point to orientate the current injected with respect to that voltage to meet active and reactive power set points) [9]. Synchronous generators, electronic power converters controlled like virtual synchronous machines (VSMs), and droop-controlled electronic converters are common realisations of grid-forming units, being the last one, probably, the most often used when electronic solutions are considered. Droop control in electronic converters mimics the reaction of synchronous machines [9] against load disturbances: they usually reduce their output frequency when the load active power increases, and they reduce their output voltage when the reactive power demand increases. Nevertheless, a different strategy may be required in the case of resistive power lines [32]. In grid-forming droop-controlled electronic converters, the frequency imposed depends on the active power injected as:

$$\omega_i = \omega_i^{ref} - m_i(P_i - P_i^{ref}) \tag{31}$$

where m_i is the droop coefficient ω_i is the converter output frequency, ω_i^{ref} is its frequency set point, P_i^{ref} is its active power set point, and P_i is the active power injected by the converter. This formulation of the droop control is valid for systems with mainly inductive impedances between units.

The main steps to design a decentralised hierarchical control for a microgrid are summarised in Fig. 2. The secondary control design follows the guidelines described in Section 3, and should be validated through dynamic simulations including lower control layers.

The tertiary control design follows the guidelines described in Section 2, and its set-point updating frequency should be such that the secondary control is able to reach a given set point before an update is provided.

4. Case study and results

The system under study is shown in Fig. 3. It consists of four agents, which are electronic grid-forming converters (DG1–DG4), some AC lines, and a DC link with two grid-following interface converters (INV1 and INV2).

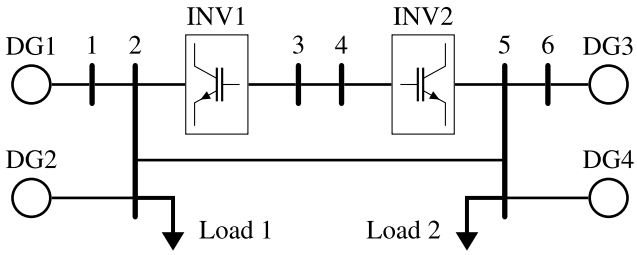

Fig. 3. 6-bus system with four generators and two loads with one point-to-point DC link between buses 2 and 5. DC/AC interface converters are named INV1 and INV2.

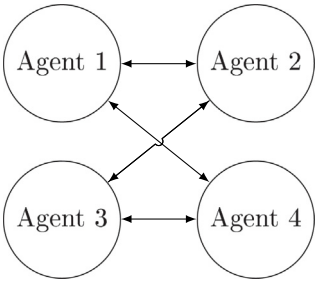

Fig. 4. Communication graph used for the decentralised economic dispatch algorithm.

The graph used for the communication among agents, shown in Fig. 4, has an adjacency matrix as follows:

$$A = \begin{bmatrix} 0 & 1 & 0 & 1 \\ 1 & 0 & 1 & 0 \\ 0 & 1 & 0 & 1 \\ 1 & 0 & 1 & 0 \end{bmatrix} \tag{32}$$

Table 2
Coefficient of the agents' cost functions and power range for every agent.

DG	c_{B_i} [$/MW]	c_{A_i} [$/MW^2]	P_{min} [MW]	P_{max} [MW]
1	2	0.04	0	80
2	3	0.03	0	80
3	4	0.035	0	80
4	4	0.03	0	80

Table 3
Communication delay implemented for each test case.

Case	Delay (ms)
I	50
II	100
III	200

Table 4
Comparison of the performance of different energy dispatch algorithms under different communication delays.

Case	Algorithm	cost [$/h]	P_{gen} [MW]
I	Centralised	994.4726	202.9
I	Triggered icost	994.4726	202.9
I	icost	994.3421	202.8805
I	Triggered base	994.4726	202.9
I	Base	0	0
II	Centralised	994.4726	202.9
II	Triggered icost	994.4726	202.9
II	icost	984.4558	201.3981
II	Triggered base	994.4726	202.9
II	Base	1904	320
III	Centralised	994.4726	202.9
III	Triggered icost	994.4726	202.9
III	icost	962.0203	198.0135
III	Triggered base	994.47	202.8996
III	Base	0	0

4.1. Convergence of the proposed decentralised economic dispatch algorithm under communication delays

This section compares the proposed method with one existing reference method in the literature, [23], under different communication delays between the agents. The objective of this section is to demonstrate the robustness to delays as the key novelty of the proposed decentralised economic dispatch algorithm.

Table 2 includes each agent's coefficients of its cost function, and minimum and maximum allowed active power. Table 3 shows the communication time delay between agents included in the simulations for each test carried out on the case study. The communication delays chosen are based on typical values in this kind of control structure [40]. The communication delay is included as a constant delay in all the communication links between agents. Since all agents have an equal convergence coefficient for the consensus ($\sum_j a_{ij}^{Ter} = \sum_k a_{ik}^{Ter} \forall\ j,k$ and $\gamma_i = \gamma_j\ \forall\ i,j$), the worst case from the stability viewpoint is when all delays are equal to the maximum value.

Fig. 5 compares the simulation results of the proposed algorithm with those of the algorithm in [23]. Non-triggered (original) and triggered versions, in both cases, are considered (see figure caption for a full explanation). A centralised algorithm has also been included for benchmarking. Table 4 includes numerical details of the results. Clearly, the original realisations of both algorithms ("icost" and "ref.") are highly affected by communication delays: "icost" reaches consensus despite communications delays but the bigger the delay, the larger the deviation of the solution from the optimum is; and "ref" fails to converge for communication delays above a certain threshold, as shown in [24]. The triggered realisations ("T. icost" and "T. ref.") are more robust. In fact, for each algorithm, the final consensus value was always reached in the same number of iterations. These iterations take longer as the communication delay grows. Nevertheless, the proposed algorithm ("T. icost") always takes fewer iterations than "T. ref." to reach consensus.

Although the proposed algorithm is less affected by communication delays, the solution obtained by the non-triggered version of the algorithm does not meet the generation-demand constraint with large communication delays.

Fig. 6 shows the evolution of the virtual cost and power set point of each agent during the consensus process for the communication delay in case I. The proposed triggered algorithm was used. Clearly, the virtual cost of all agents evolves to a consensus value. In fact, this value is the marginal cost of all non-limited units at the optimal solution.

4.2. Performance and robustness of the proposed secondary control in the case study

The parameters used for the microgrid and converter models in Fig. 3 are included in Appendix C. The control structure for interface converters INV1 and INV2 is shown in Figs. C.16 and C.17. The control structure for grid-forming converters DG1–4 is shown in Fig. C.18. The parameters used for the system model are shown in Table C.6.

For simplicity, the communication graph used for the secondary control is the same as the one used for the economic dispatch, with DG1 set as the leader at the beginning of the simulation. Adjacent matrices are:

$$A^P = A^Q = A^\omega = \begin{bmatrix} 0 & 1 & 0 & 1 \\ 1 & 0 & 1 & 0 \\ 0 & 1 & 0 & 1 \\ 1 & 0 & 1 & 0 \end{bmatrix} \tag{33}$$

In this particular application, voltage consensus is not implemented; therefore:

$$A^v = \mathbf{0}^{4\times4} \tag{34}$$

Non-linear electromagnetic dynamic simulations of the microgrid shown in Fig. 3 were carried out to evaluate the proposed secondary control and its robustness.

The MATLAB-Simulink tool VFlexP, described in [49] was used to build the dynamic model of the microgrid and for simulations.

The dynamic models used were initialised from the power flow solution of the hybrid microgrid obtained using the flexible universal branch model in [13], an extension of MATPOWER [50].

The robustness of the secondary control structure to communication time delays and loss of communication links was investigated by modal analysis (with a linear model of the delay) and non-linear simulation (with an exact delay), respectively.

Fig. 7 shows how the eigenvalues of a linear approximation of the system model move when the communication delay between agents is varied from 50 to 200 ms in 100 equal steps. The communication delay is modelled by a 3rd-order Padé approximation when linearising the system equations, as suggested in [38]. The same delay was applied in all communication channels. As stated in [40], although the communication delay is stochastic in real scenarios, a constant modelling of the delay as its average value is enough for this type of stability studies.

Eigenvalues are shown in Fig. 7 which includes the phase ($\angle\lambda_i$) and magnitude ($|\lambda_i|$) of eigenvalues. The latter is shown in a *log* scale to include eigenvalues with very large magnitude and those with a small one, in the same figure. In the case of complex conjugates, only the eigenvalue with a positive imaginary part has been plotted ($\mathrm{Imag}(\lambda_i) > 0$). In this representation, if all eigenvalues have a phase between 90 and 270 degrees (i.e., they are in the left-hand side of the complex plane), the system is stable. It should be noticed that the linearisation of the non-linear system for this modal analysis stability study is done for a specific operation point. If the operation point changes (for example,

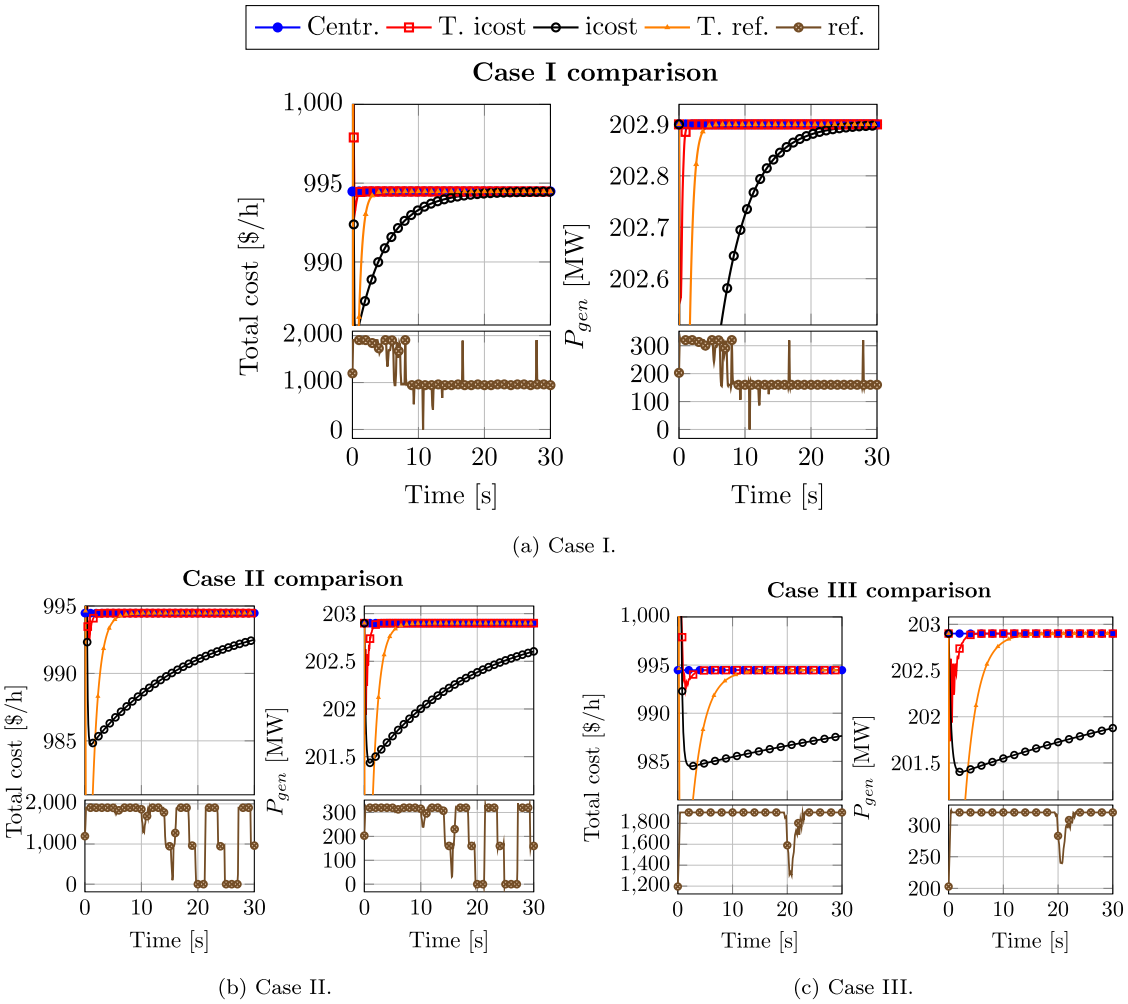

(a) Case I.

(b) Case II.

(c) Case III.

Fig. 5. Comparison of the convergence evolution of the objective function (global operation cost) and the power balance obtained using the different approaches for cases I, II and III. "Centr." stands for the conventional centralised approach, "T. icost" stands for the triggered version of the proposed approach, "icost" stands for the non-triggered version of the proposed approach, "ref." stands for the approach presented in [23] (note that this last approach is shown separately in the lower part of each graph due to the large differences in the Y-axis values), and "T. ref." modifies that proposal to include a triggered approach.

changing the active-power dispatch), the linear system will not be exactly the same.

Fig. 7 shows that the system remains stable for the range of the communication delay tested. However, some complex eigenvalues move closer to the stability limit ($\angle\lambda_i = 90^o$) when increasing the communication delay. If the delay is increased further, the system could become unstable. This could be avoided if the delay can be compensated somehow [40]. In this work, we propose slowing down the secondary control until the stability of the system is not affected by the expected communication time delays. A constant 100 ms delay is used for all communication links in the remaining case studies in this paper unless otherwise stated. Incidentally, the delay will not affect the tertiary control layer convergence as long as the "triggered" version is used.

To test the robustness of the proposed secondary control against the loss of communication links among agents, the system response to a 5.85% reduction in both loads of the system is compared in three scenarios:

1. No link loss (as in Fig. 4).
2. The links starting at DG2 are lost.
3. The links starting at DG2 and the links starting at DG4 are lost.

Table 5 includes the Laplacian (L matrix) and its eigenvalues for the communication graphs corresponding to the three scenarios considered.

Table 5
Eigenvalues of the Laplacian matrix for each communication graph case of the communication link loss study.

Case	$L = L^{\omega} + G^{\omega}$	L eig.
1	$\begin{bmatrix} 3 & -1 & 0 & -1 \\ -1 & 2 & -1 & 0 \\ 0 & -1 & 2 & -1 \\ -1 & 0 & -1 & 2 \end{bmatrix}$	$\begin{bmatrix} 0.1864 \\ 2 \\ 2.4707 \\ 4.3429 \end{bmatrix}$
2	$\begin{bmatrix} 2 & 0 & 0 & -1 \\ -1 & 2 & -1 & 0 \\ 0 & 0 & 1 & -1 \\ -1 & 0 & -1 & 2 \end{bmatrix}$	$\begin{bmatrix} 0.1981 \\ 1.555 \\ 2 \\ 3.247 \end{bmatrix}$
3	$\begin{bmatrix} 1 & 0 & 0 & 0 \\ -1 & 2 & -1 & 0 \\ 0 & 0 & 0 & 0 \\ -1 & 0 & -1 & 2 \end{bmatrix}$	$\begin{bmatrix} 0 \\ 1 \\ 2 \\ 2 \end{bmatrix}$

Only the third case has an L matrix with one zero eigenvalue, and consensus is not guaranteed.

Fig. 8 includes the simulation results of the dynamic response of the active power of DGs 1–4 to a 5.85% reduction in both loads for the three case scenarios considered.

Clearly, results show that consensus is not reached in the third case, confirming the theoretical foundations (i.e., consensus is only

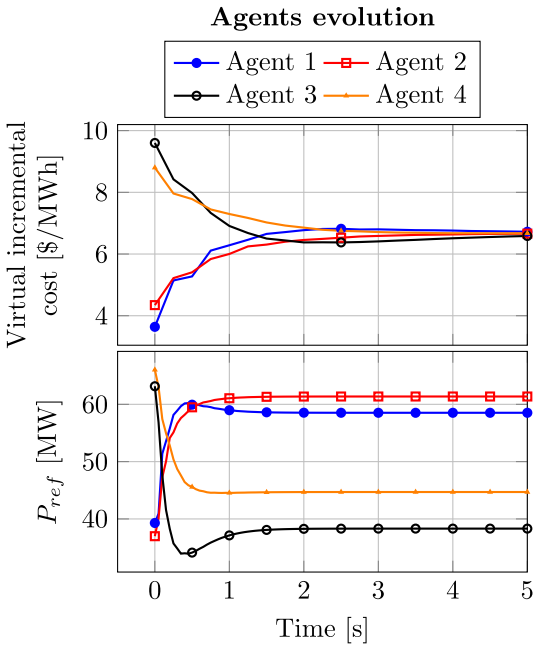

Fig. 6. Evolution of the virtual cost and power set point of each agent during the consensus process for the communication delay on case I.

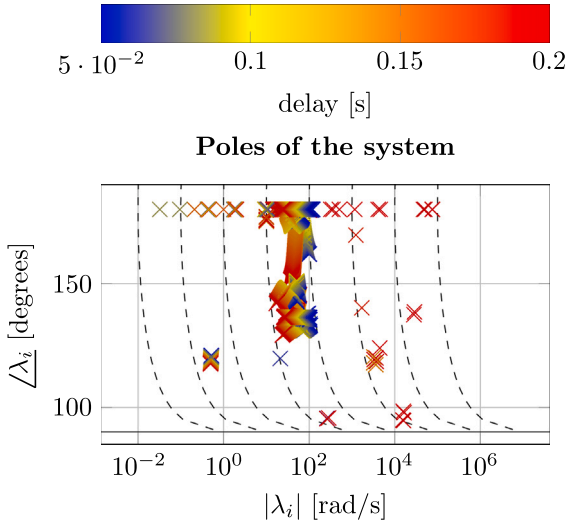

Fig. 7. Variation of the system eigenvalues λ_i when the constant communication delay between agents is varied from 50 to 200 ms. The figure includes the phase and magnitude of eigenvalues. The latter is shown in a *log* scale to include eigenvalues with very large magnitude and those with a small one, in the same figure.

guaranteed if the conditions for the Laplacian eigenvalues described in Appendix B are met).

Fig. 9 includes the simulation results of the dynamic response of the active power of DGs 1–4 to the outage of DG4 for the three case scenarios considered.

Again, results show that consensus is reached in the first and second cases, but not reached in the third case, confirming the theoretical foundations.

To test the performance of the proposed secondary control in cases of deviations from the set-point dispatched by the tertiary control layer, it is also tested under demand variations. Fig. 10 shows the cost increment from the optimal operating point (i.e., updating the tertiary

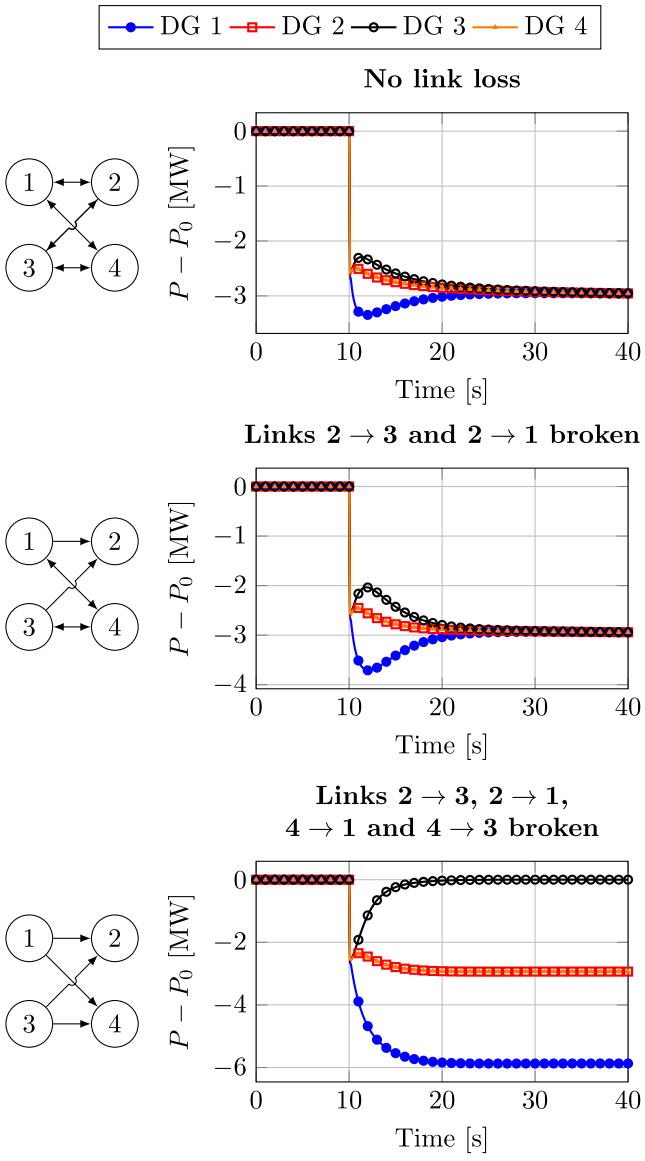

Fig. 8. Active power response of DGs 1–4 to a 5.85% reduction in both loads for each communication graph case of the communication link loss study.

control set points for the active power after each load disturbance) in the operation of the proposed secondary control under demand variations from the initially dispatched point. The cost increment is calculated as the cost obtained with the proposed method minus the cost of the optimal dispatch at the same operation point. Results with a secondary control based on active power sharing (*Default SecC*) are compared with those of a cost-based secondary control (*Cost-based SecC*) in that figure.

As expected, Fig. 10 shows that the cost-based secondary control is always cheaper than the one based on active power sharing. However, the cost increment in both methods is small for the tests carried out, even in cases with an active power demand that is very different from the scheduled one. In these cases, the tertiary control layer should update the active power set points.

To evaluate the performance of the proposed hierarchical control, the active power consumption of both loads in Fig. 3 is varied. First of all, it is reduced to 0.05% of the original load and then increased up to 140% of the original load. For simplicity, the load is changed linearly every 20 s for 3600 s (1 h). The costs are varied randomly with

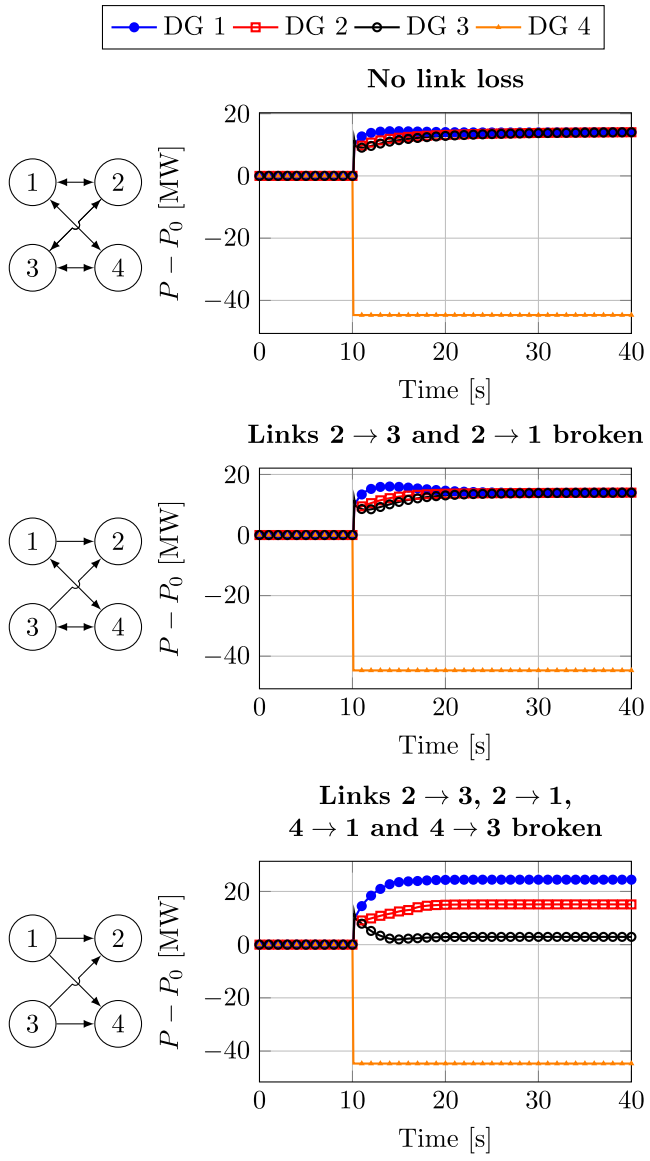

Fig. 9. Active power response of DGs 1–4 to the outage of DG4 for each communication graph case of the communication link loss study.

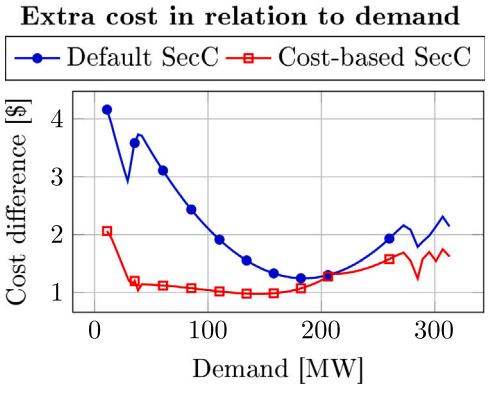

Fig. 10. Cost increment from the optimal one, with a secondary control based on active power sharing (*Default SecC*) and with a cost-based secondary control (*Cost-based SecC*), as demand varies.

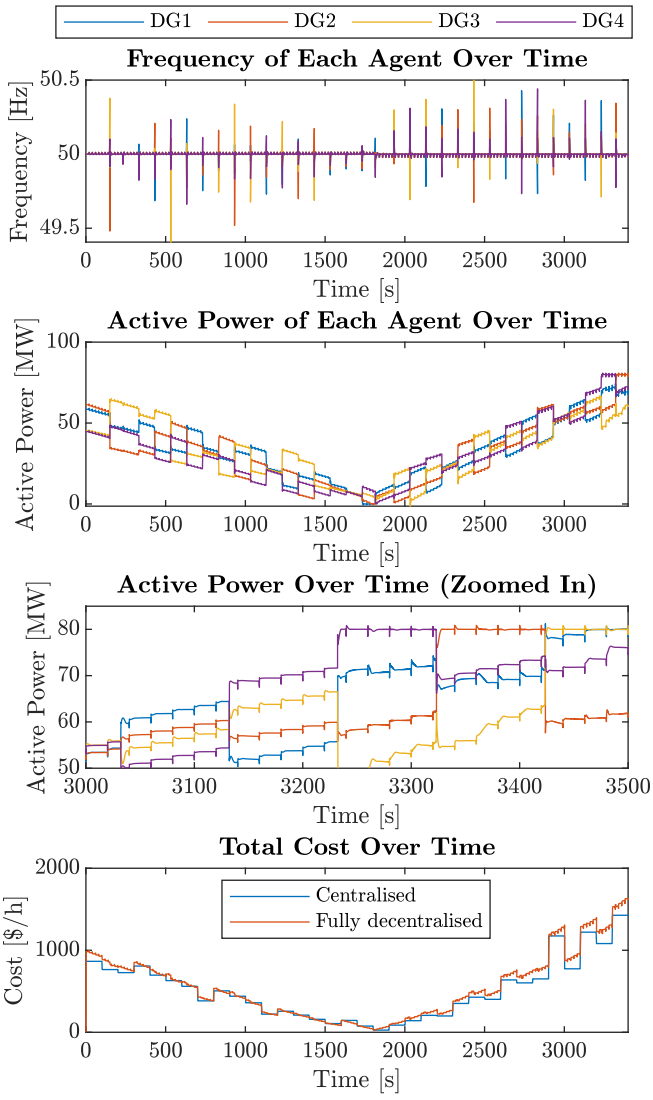

Fig. 11. System performance under demand variation.

a uniform distribution between 2 and 4 for c_{B_i} and between 0.02 and 0.04 for c_{A_i} every 100 s, time when also the tertiary control updates the active-power set points. The communication graph used here is the one presented in Fig. 4, with the same adjacency matrix.

Fig. 11 shows the active power injected by DGs 1–4 during the test.

As clearly shown for the active power results in Fig. 11, the saturation of the active power set points works properly. The proposed secondary control structure also manages to recover the frequency to its nominal value after each active load disturbance.

The differences between the scheduled, and real active and reactive powers are shared by all DGs depending on the a_{ij}^P and a_{ij}^Q coefficients, respectively. In the case of the active power, as described in Section 3.1, a_{ij}^P coefficients are modified to consider unit costs in the secondary control layer.

4.3. Real-time validation of the proposed fully decentralised hierarchical control

For the real-time validation of the proposed fully decentralised hierarchical control, the algorithm was implemented in a real-time simulator, OPAL-RT OP4510. The process followed for the real-time simulation of the proposed algorithm is depicted in Fig. 12. The nonlinear system was modelled using MATLAB Simulink and compiled for

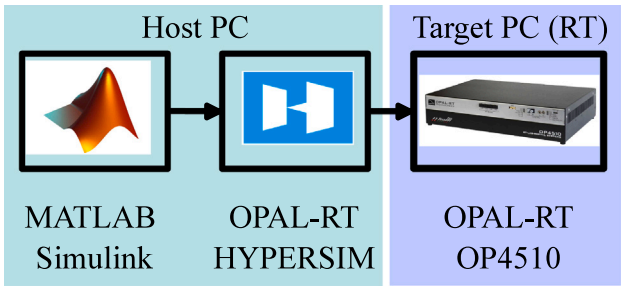

Fig. 12. Diagram of the process for the real-time simulation of the proposed hierarchical control in the OPAL-RT OP4510 simulator. The model of the system is implemented in MATLAB-Simulink, and then it is compiled for OPAL-RT HYPERSIM software. Then, the HYPERSIM model is executed in real time on the OP4510.

OPAL-RT HYPERSIM software. Then, the HYPERSIM model is executed in real time on the OP4510. The time step was set to 50 μs, the performance factor was set to 1 and the processor load level was set to 0.8.

The usage of a single core of the OPAL-RT OP4510 for this real-time simulation was around 5%. The real-time simulation results are shown in Fig. 13.

Regarding the tertiary control, as clearly shown in the figure, the virtual marginal costs reach consensus in a few seconds at every dispatch.

This means that the economic dispatch converges in a few seconds, and that an optimal solution is found, since all the virtual marginal costs are equal after convergence.

Regarding the secondary control, the voltage and frequency recover their nominal values in a few seconds after each disturbance. The reactive power sharing is set equal to all converters except DG1. The active power sharing of disturbances depends on:

1. The active-power set point set by the decentralised economic dispatch problem.
2. The disturbances (deviations) from the dispatched active-power set points are shared depending on the costs, as defined by (30), which can help to understand the deviations from the dispatched set points.

Noticed that the active power injected has a mismatch with the dispatched one. This deviation is caused on purpose, because the demand is changed before the update of the tertiary control set-points to test the performance of the proposed secondary control layer.

Fig. 13 also shows that the total operation cost is close to the "Optimal Cost" which is the total cost the system would have with a centralised dispatch immediately after every load and cost change.

5. Large case study

This section includes the validation of the proposed decentralised hierarchical control structure for a larger case study to prove its scalability. The large case study implemented in this section is the connection of the IEEE 57-bus system and the IEEE 14-bus system with a 10-bus DC system. The system includes 12 grid-forming converters that are agents involved in the proposed hierarchical control. This is essentially the same system implemented in [49] with two extra lines (line connecting buses 150 and 204 and line connecting buses 151 and 205) with very small impedance ($x_l = 4 \cdot 10^{-4}$ pu and $r_l = 10^{-4}$ pu) to have only one synchronous AC area. Fig. 14 depicts the system studied. Buses with generators are highlighted in red.

The adjacency matrix of this system with 12 agents follows a ring structure and is implemented in MATLAB as:

$$A = 0.5 * circshift(eye(12), 1) + 0.5 * circshift(eye(12), -1); \quad (35)$$

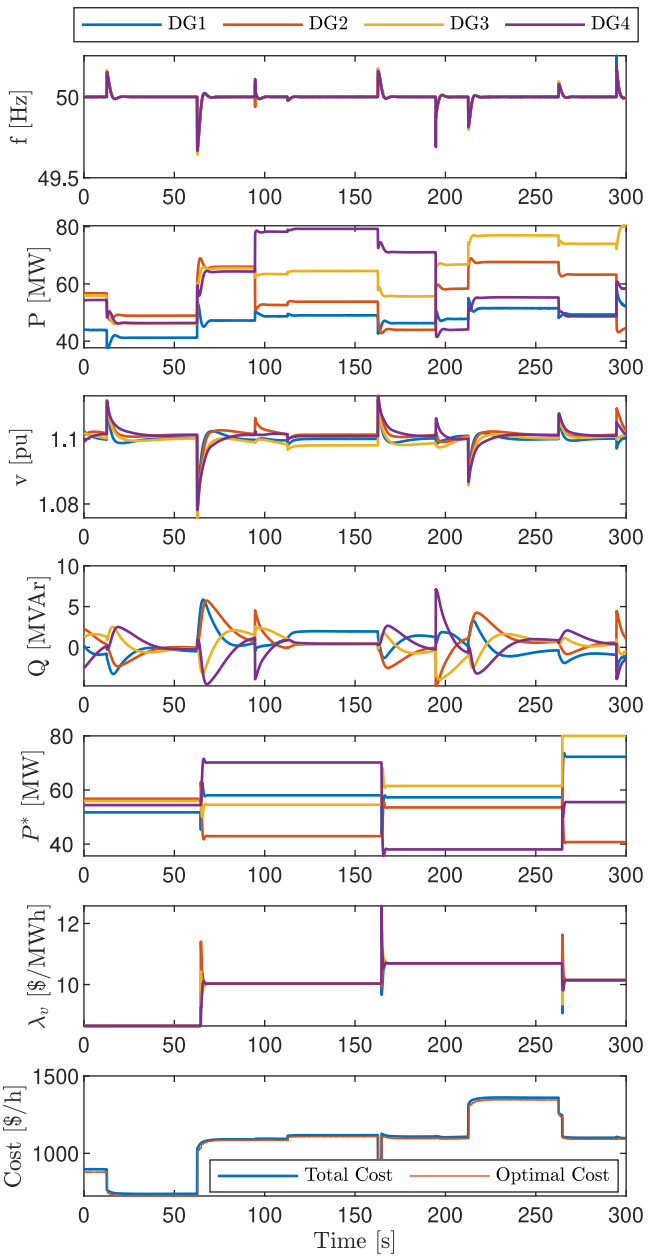

Fig. 13. Results of the real-time validation of the proposed decentralised hierarchical control.

which gives a symmetrical 12 × 12 matrix with all diagonal elements equal zero and with its upper part as:

$$\begin{cases} A(i, i+1) = 0.5, \ i = 1, \ldots, 11 \\ A(1, 12) = 0.5 \end{cases} \quad (36)$$

Modal analysis, similar to the one conducted in Fig. 7, demonstrates that the proposed secondary control is stable with the tested conditions and parameters. Details on the secondary control implementation can be found in [51]. A similar simulation to the one shown in Fig. 11 (i.e., with MATLAB, changing demand and costs) was carried out for this system, and the results are shown in Fig. 15. Results demonstrate that the proposed decentralised hierarchical control is functioning effectively. The proposed secondary control structure successfully restores the frequency to its nominal value after active load disturbances. The differences between the scheduled active and reactive powers and the actual values are shared among all DGs using the

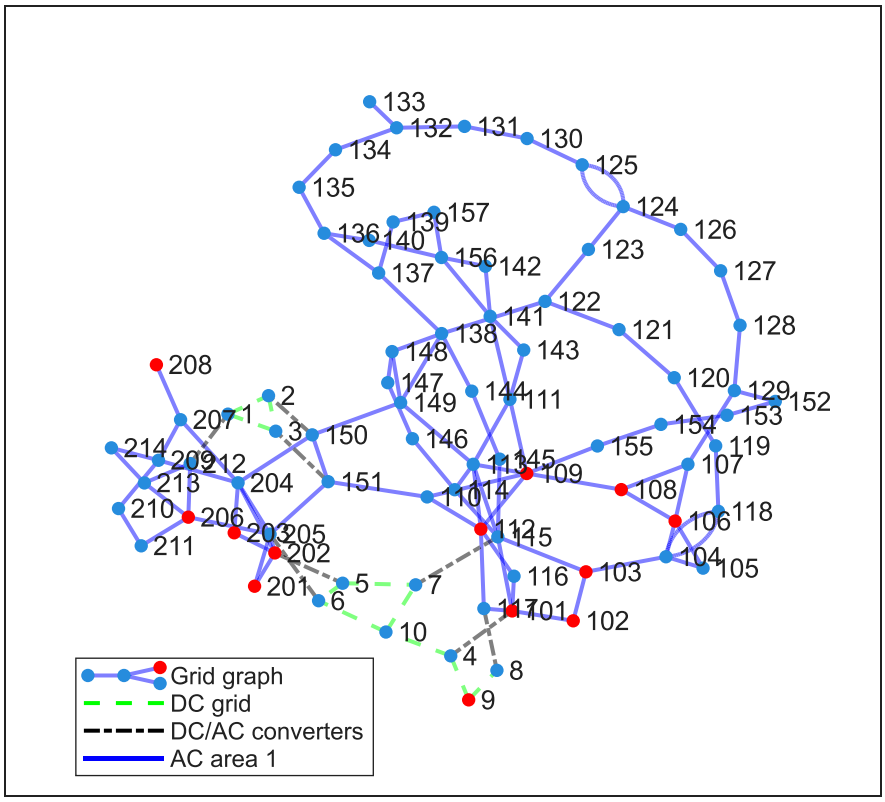

Fig. 14. IEEE 57-bus system connected to the IEEE 14-bus system and a 10-bus DC system.

coefficients a_{ij}^{P} and a_{ij}^{Q}. Again, the a_{ij}^{P} coefficients are adjusted in the secondary control layer to reflect unit costs. As shown in the figure, the proposed fully decentralised hierarchical control achieves an operation cost close to the optimal one, named "Centralised" in the figure.

6. Conclusion and future work

This paper proposes a fully decentralised multi-agent hierarchical control of a hybrid AC–DC microgrid and illustrates its performance. The secondary and tertiary control layers of the proposed control are based on consensus formulation. The tertiary control layer proposed calculates the optimal active-power sharing between generators in the microgrid cooperatively in a decentralised manner. The convergence of this control layer is not affected by the communication delay thanks to the proposed triggered scheme. The results obtained by the proposed algorithm are compared against an existing decentralised approach and against the conventional centralised solution. Simulation results prove the robustness of the proposed method to communication delays. The secondary control layer proposed manages the active-power sharing of the deviations from the dispatched operation point. Simulation results show the performance of the proposed control, which considers active-power limits for the generators and is able to include unit costs in the secondary control layer.

Future work will focus on considering the grid and voltage and reactive-power control on the economic dispatch problem and extending the algorithm to solve a multi-period decentralised economic dispatch problem, considering energy storage characteristics such as degradation and state of charge. On the secondary control layer, future research will include the design of a trigger mechanism for the proposed incremental secondary control.

CRediT authorship contribution statement

Andrés Tomás-Martín: Writing – original draft, Visualization, Validation, Software, Methodology, Data curation, Conceptualization. **Behzad Kazemtabrizi:** Writing – review & editing, Validation, Supervision, Resources, Data curation. **Aurelio García-Cerrada:** Writing – review & editing, Validation, Supervision, Resources, Project administration. **Lukas Sigrist:** Writing – review & editing, Validation, Supervision, Resources, Data curation. **Emilio J. Bueno:** Writing – review & editing, Supervision, Project administration.

Declaration of competing interest

The authors declare that they have no known competing financial interests or personal relationships that could have appeared to influence the work reported in this paper.

Acknowledgements

This work has been partially financed by the project TED2021-130610B-C22, funded by MCIN/AEI/10.13039/501100011033, and by the European Union NextGenerationEU/PRTR. The collaboration between Durham University and Comillas has been eased with a special grant "for research-staff mobility to foreign research centres" to Andrés Tomás-Martín, from Comillas Pontifical University.

Appendix A. Proof of convergence of the proposed decentralised economic dispatch problem using a Lyapunov function

The objective of this section is to demonstrate that the consensus formulation on Eqs. (10)–(12) converges to the optimal solution and minimises the global cost:

$$J\left(P^{*}\right)=\sum_{i\in N}\left(c_{A_i}\left(P_i^{*}\right)^2+c_{B_i}P_i^{*}+c_{C_i}\right) \tag{A.1}$$

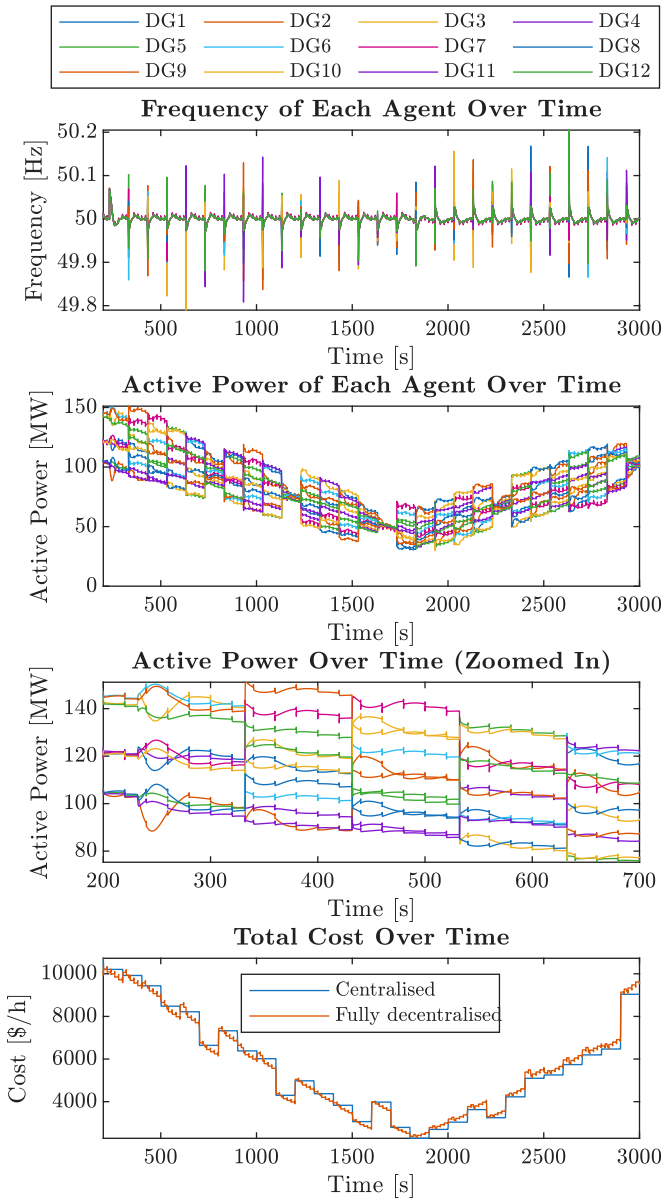

Fig. 15. Performance of the proposed hierarchical control under cost and demand variation in a large system.

where the marginal cost of each agent is:

$$\lambda_i(t) = \frac{\partial J}{\partial P_i^*} = 2c_{A_i} P_i^*(t) + c_{B_i} \tag{A.2}$$

Let us consider the following scalar function:

$$W(t) = \frac{1}{2} \sum_{i \in N} \sum_{j \in N} a_{ij}^{\text{Ter}} \left[\lambda_i(t) - \lambda_j(t)\right]^2 \tag{A.3}$$

1. $W(t) > 0$ always, unless $\lambda_i(t) = \lambda_j(t) = \lambda^*$ for all connected generators (graph nodes)
2. λ^* will be the optimal solution for the microgrid at one "equilibrium point".
3. Furthermore,

$$\frac{dW}{dt} = \sum_{i \in N} \sum_{j \in N} a_{ij}^{\text{Ter}} \left(\lambda_i - \lambda_j\right)\left(\dot{\lambda}_i - \dot{\lambda}_j\right) \tag{A.4}$$

where

$$\dot{\lambda}_i = 2c_{A_i} \frac{dP_i^*(t)}{dt} \tag{A.5}$$

which becomes:

$$\dot{\lambda}_i = 2c_{A_i}\gamma_i \sum_{k \in N} a_{ik}^{\text{Ter}} \left(\lambda_k - \lambda_i\right) \tag{A.6}$$

Calling,

$$\delta_i = \sum_{k \in N} a_{ik}^{\text{Ter}} \left(\lambda_i - \lambda_k\right) \tag{A.7}$$

yields,

$$\dot{\lambda}_i = -2c_{A_i}\gamma_i\delta_i \tag{A.8}$$

and taking this result to (A.4):

$$\frac{dW}{dt} = \sum_{i \in N} \sum_{j \in N} a_{ij}^{\text{Ter}} \left(\lambda_i - \lambda_j\right)\left(2c_{A_j}\gamma_j\delta_j - 2c_{A_i}\gamma_i\delta_i\right) \tag{A.9}$$

In other words:

$$\frac{dW}{dt} = -2 \sum_{i \in N} c_{A_i}\gamma_i\delta_i \sum_{j \in N} a_{ij}^{\text{Ter}} \left(\lambda_i - \lambda_j\right) + 2 \sum_{j} c_{A_j}\gamma_j\delta_j \sum_{i \in N} a_{ij}^{\text{Ter}} \left(\lambda_i - \lambda_j\right) \tag{A.10}$$

and

$$\frac{dW}{dt} = -2 \sum_{i \in N} c_{A_i}\gamma_i\delta_i^2 - 2 \sum_{j \in N} c_{A_j}\gamma_j\delta_j^2 = -4 \sum_{i \in N} c_{A_i}\gamma_i\delta_i^2 \tag{A.11}$$

4. Since $\gamma_i > 0$, $\delta_i^2 \geq 0$ and $c_{A_i} > 0\ \forall i$, $dW/dt \leq 0$, $W(t)$ has proved to be a Lyapunov function that guarantees that $\lambda_i(t) = \lambda_j(t) = \lambda^*$, $\forall\ i\&j$, is a stable equilibrium point and all generator units will reach the consensus solution, eventually.

Appendix B. Proof of convergence of the incremental secondary control using a Lyapunov function

Let us define,

- the state vector:

$$\Delta\omega^{\text{ref}} = \left[\Delta\omega_1^{\text{ref}}, \Delta\omega_2^{\text{ref}}, \ldots, \Delta\omega_n^{\text{ref}}\right]^T \tag{B.1}$$

- the Laplacian matrix (L^ω) of the graph:

$$L^\omega = D^\omega - A^\omega \tag{B.2}$$

where A is the adjacency matrix, and D is the in-degree matrix whose elements are defined as:

$$d_{ii}^\omega = \sum_{\forall j \in N} a_{ij}^\omega \tag{B.3}$$

- and the pinning matrix of the graph as:

$$G^\omega = \text{diag}\left(g_1^\omega, g_2^\omega, \ldots, g_n^\omega\right) \tag{B.4}$$

One can rewrite the consensus in Eq. (22) in matrix form as:

$$\frac{d\Delta\omega^{ref}}{dt} = -\left(L^\omega + G^\omega\right)\Delta\omega^{ref} = -L\Delta\omega^{ref} \tag{B.5}$$

where $L = L^\omega + G^\omega$.

The following candidate for a Lyapunov function can be proposed:

$$J\left(\Delta\omega^{ref}\right) = \frac{1}{2}\left(\Delta\omega^{ref}\right)^T \cdot M \cdot \Delta\omega^{ref} \tag{B.6}$$

where $J\left(\Delta\omega^{ref}\right)$ is positive for $\Delta\omega^{ref} \neq 0$ and $J(0) = 0$, if matrix M is positive definite [52].

Table C.6
Parameters used for the simulation of the microgrid.

Grid-forming converters			
m_P	0.05 pu	n_Q	0.05 pu
R_f	0.01 pu	L_f	0.1 pu
C_f	0.1 pu	R_{cf}	1000 pu
R_c	0.05 pu	L_c	0.5 pu
K_{PV}	1	K_{IV}	10
K_{PC}	1	K_{IC}	10
F_i	1	LPF_{const}	0.01 s
Interface converters			
R_{f_1}	0.0001 pu	L_{f_1}	0.15 pu
R_{f_2}	0.0002 pu	L_{f_2}	0.35 pu
K_{PC}	1	K_{IC}	10
$K_{P,PLL}$	1	$K_{I,PLL}$	20
$\alpha_{1,2}$	0.0001	$\beta_{1,2}$	0.015
γ_1	0.2	γ_2	0.2
$K_{P,DC,2}$	0.5	$K_{I,DC,2}$	10
Lines			
$R_{1\to2}$	0.001 pu	$L_{1\to2}$	0.1 pu
$R_{2\to5}$	0.05 pu	$L_{2\to5}$	0.5 pu
$R_{3\to4}$	0.05 pu	$L_{3\to4}$	0 pu
$R_{5\to6}$	0.001 pu	$L_{5\to6}$	0.1 pu
Loads			
P_{load_1}	122.9 MW	Q_{load_1}	0.3 MVAr
P_{load_2}	80 MW	Q_{load_2}	0.5 MVAr

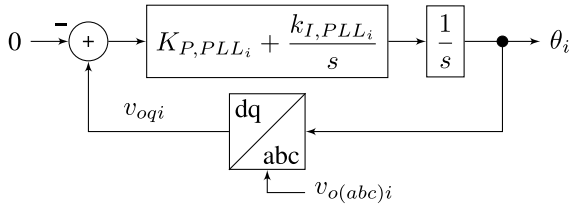

Fig. C.16. Block diagram of the phase-locked-loop.

At the same time, the derivative of $J\left(\Delta\omega^{ref}\right)$ is:

$$\begin{aligned}\frac{dJ}{dt} &= \frac{1}{2}\left[(\Delta\omega^{ref})^T M\frac{d\Delta\omega^{ref}}{dt} + \left(\frac{d\Delta\omega^{ref}}{dt}\right)^T M\Delta\omega^{ref}\right] \\ &= \frac{1}{2}\left[(\Delta\omega^{ref})^T M(-L\Delta\omega^{ref}) - (L\Delta\omega^{ref})^T M\Delta\omega^{ref}\right] \\ &= -\frac{1}{2}(\Delta\omega^{ref})^T(ML + L^T M)\Delta\omega^{ref}\end{aligned} \tag{B.7}$$

Consensus is guaranteed if matrix $(ML + L^T M)$ is positive definite so that $dJ/dt \le 0$. $(ML + L^T M)$ is positive definite, and $J\left(\Delta\omega^{ref}\right)$ is a Lyapunov function, when $L = (L^\omega + G^\omega)$ has all its eigenvalues (λ_i) with positive real part $(\lambda_i > 0\ \forall\ i)$.

Similarly, one can demonstrate the convergence of (25) and (24) given that v_i and Q_i are directly affected by v_i^{ref} and Q_i^{ref}, respectively.

The convergence of (23) can also be demonstrated providing that the system maintains synchronism (in steady state $\omega_i = \omega_j\ \forall\ i, j$).

Appendix C. Model and parameters of the test system

This section describes the models used for the analysis and simulation of the proposed decentralised hierarchical control. Full details on the models can be found in [51].

Table C.6 includes the parameters used for the microgrid and converter models.

The interface DC/AC converters INV1 and INV2 in Fig. 3 are controlled as grid-following converters on the AC side.

The active-power losses involved in the conversion are modelled as:

$$P_{loss,i} = \alpha_i + \beta_i P_i^{AC} + \gamma_i (P_i^{AC})^2 \tag{C.1}$$

Tagged signals:
{1} $\mathbf{v}_{ii}^*$ is the voltage set by the converter before the inductance.
{2} $\mathbf{i}_{oi}$ is the current through the inductance.
{3} $\mathbf{v}_{oi}$ is the voltage of the point of connection.

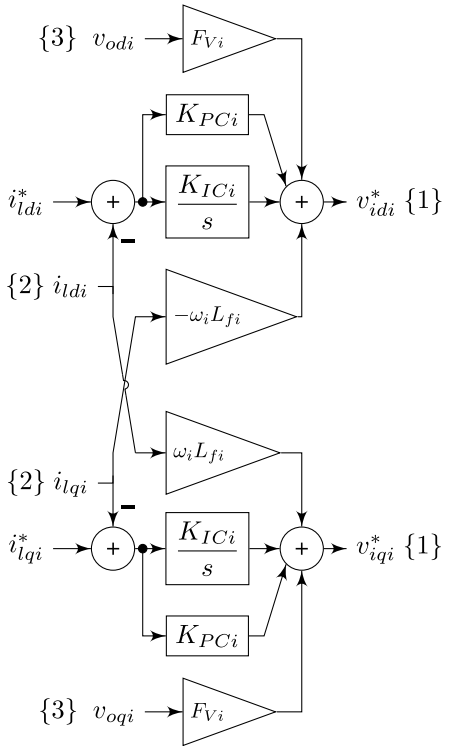

Fig. C.17. Current controller of one grid-following converter.

As grid-following converters, they track the voltage amplitude and angle of their AC point of connection and orientate their injected current with respect to that voltage to meet active and reactive power requirements. This tracking is done with a phase-locked loop and Park's transform, as shown in Fig. C.16. Park's transform is a well-known reference frame transformation from 3-phase magnitudes into constant values in the steady state.

As shown in Fig. C.17, direct (d-) and quadrature (q-) axis currents of the grid-following converters are controlled with PI controllers, after Park's transform, and the d–q coupling terms are compensated.

Set points for d- and q-axis currents are calculated using d- and q-axis voltages (v_{odi}, v_{oqi}) measured at the point of connection, and the active and reactive power set points P_i^{ref} and Q_i^{ref}:

$$i^*_{ldi} = \frac{v_{odi}P_i^{ref} + v_{oqi}Q_i^{ref}}{v_{odi}^2 + v_{oqi}^2} \tag{C.2}$$

$$i^*_{lqi} = \frac{v_{oqi}P_i^{ref} - v_{odi}Q_i^{ref}}{v_{odi}^2 + v_{oqi}^2} \tag{C.3}$$

The active and reactive power set points P_i^{ref} and Q_i^{ref} for INV1 and the reactive power set point for INV2 are kept constant and equal to the ones obtained with the power flow calculated at the operating point.

The active power reference for INV2 is modified with a PI controller to maintain its DC voltage:

$$P_2^{ref}(s) = (v_{DC,2} - v_{DC,2}^{ref})\left(K_{P,DC,2} + \frac{K_{I,DC,2}}{s}\right) \tag{C.4}$$

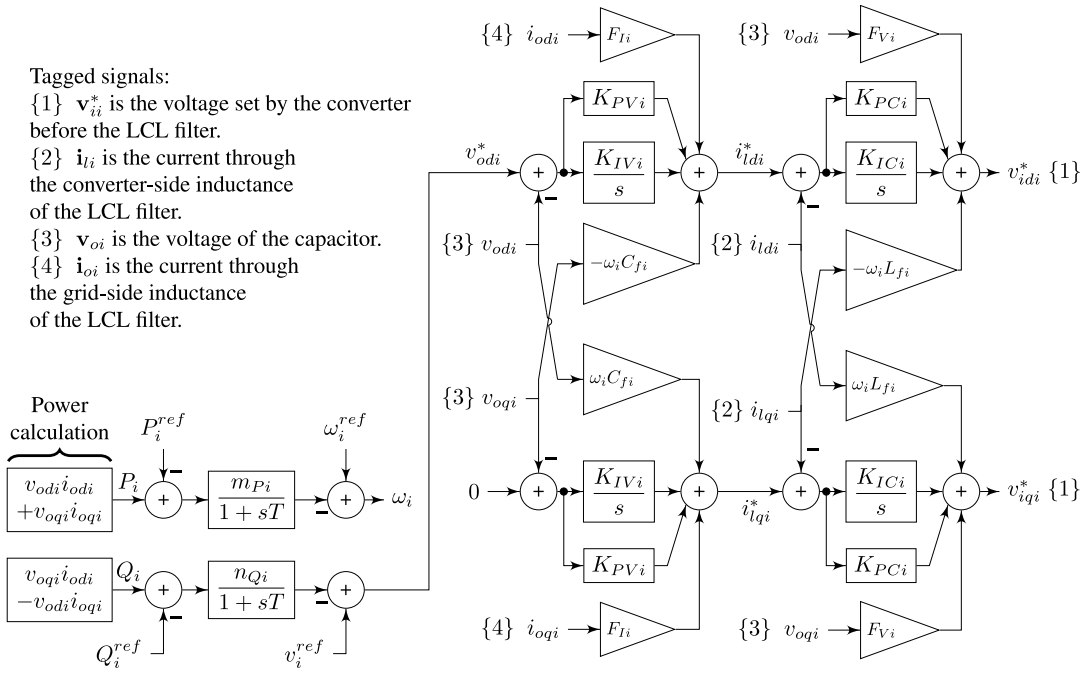

Fig. C.18. Primary control (droop control) and voltage and current controllers of one grid-forming converter.

DGs 1–4 are grid-forming converters working with droop control. Fig. C.18 depicts the control diagram of the primary control (droop control) and voltage and current controllers of one grid-forming converter.

Data availability

The data and models used are available in the GitHub repository "VFlexP", included in the reference list.

References

[1] Marnay C, Chatzivasileiadis S, Abbey C, Iravani R, Joos G, Lombardi P, Mancarella P, von Appen J. Microgrid evolution roadmap. In: 2015 international symposium on smart electric distribution systems and technologies. Vienna, Austria: IEEE; 2015, p. 139–44.

[2] Louassaa K, Guerrero JM, Boukerdja M, Chouder A, khan B, Cherifi A, Yousaf MZ. A novel hierarchical control strategy for enhancing stability of a DC microgrid feeding a constant power load. Sci Rep 2025;15(1):7061.

[3] Bidram A, Davoudi A. Hierarchical structure of microgrids control system. IEEE Trans Smart Grid 2012;3(4):1963–76.

[4] Guerrero JM, Vasquez JC, Matas J, de Vicuna LG, Castilla M. Hierarchical control of droop-controlled AC and DC microgrids—A general approach toward standardization. IEEE Trans Ind Electron 2011;58(1):158–72.

[5] Conejo A, Aguilar MJ. Secondary voltage control: nonlinear selection of pilot buses, design of an optimal control law, and simulation results. IEE Proc - Gener Transm Distrib 1998;145(1):77–81.

[6] Khayat Y, Shafiee Q, Heydari R, Naderi M, Dragicevic T, Simpson-Porco JW, Dorfler F, Fathi M, Blaabjerg F, Guerrero JM, Bevrani H. On the secondary control architectures of AC microgrids: An overview. IEEE Trans Power Electron 2020;35(6):6482–500.

[7] Hatziargyriou N. Microgrids: Architectures and control. Chichester, United Kingdom: IEEE Press-Wiley; 2014.

[8] Chang J-W, Park J-Y, Hwang P-I. Decentralized secondary control of DGs for an islanded hybrid AC/DC Microgrid. IEEE Access 2024;12:3597–610.

[9] Bidram A, Davoudi A, Lewis FL. A multiobjective distributed control framework for islanded AC microgrids. IEEE Trans Ind Informatics 2014;10(3):1785–98.

[10] Rajabdorri M, Kazemtabrizi B, Troffaes M, Sigrist L, Lobato E. Inclusion of frequency nadir constraint in the unit commitment problem of small power systems using machine learning. Sustain Energy, Grids Networks 2023;36:101161.

[11] Happ H. Optimal power dispatch - A comprehensive survey. IEEE Trans Power Appar Syst 1977;96(3):841–54.

[12] Poolla BK, Hota AR, Bolognani S, Callaway DS, Cherukuri A. Wasserstein distributionally robust look-ahead economic dispatch. IEEE Trans Power Syst 2021;36(3):2010–22.

[13] Alvarez-Bustos A, Kazemtabrizi B, Shahbazi M, Acha-Daza E. Universal branch model for the solution of optimal power flows in hybrid AC/DC grids. Int J Electr Power Energy Syst 2021;126:106543.

[14] Capitanescu F. Critical review of recent advances and further developments needed in AC optimal power flow. Electr Power Syst Res 2016;136:57–68.

[15] Chen W, Li T. Distributed economic dispatch for energy internet based on multiagent consensus control. IEEE Trans Autom Control 2021;66(1):137–52.

[16] Roald LA, Pozo D, Papavasiliou A, Molzahn DK, Kazempour J, Conejo A. Power systems optimization under uncertainty: A review of methods and applications. Electr Power Syst Res 2023;214:108725.

[17] Tu H, Du Y, Yu H, Meena S, Lu X, Lukic S. Distributed economic dispatch for microgrids tracking ramp power commands. IEEE Trans Smart Grid 2023;14(1):94–111.

[18] Han L, Morstyn T, McCulloch M. Incentivizing prosumer coalitions with energy management using cooperative game theory. IEEE Trans Power Syst 2019;34(1):303–13.

[19] Cruz Victorio ME, Kazemtabrizi B, Shahbazi M. Real-time resilient microgrid power management based on multi-agent systems with price forecast. IET Smart Grid 2022;6(2):190–204.

[20] Zhou X, Ma Z, Zou S, Zhang J. Consensus-based distributed economic dispatch for multi micro energy grid systems under coupled carbon emissions. Appl Energy 2022;324:119641.

[21] Binetti G, Davoudi A, Lewis FL, Naso D, Turchiano B. Distributed consensus-based economic dispatch with transmission losses. IEEE Trans Power Syst 2014;29(4):1711–20.

[22] Zhang Z, Chow M-Y. Incremental cost consensus algorithm in a smart grid environment. In: 2011 IEEE power and energy society general meeting. 2011, p. 1–6.

[23] Yang S, Tan S, Xu J-X. Consensus based approach for economic dispatch problem in a smart grid. IEEE Trans Power Syst 2013;28(4):4416–26.

[24] Zhao C, Duan X, Shi Y. Analysis of consensus-based economic dispatch algorithm under time delays. IEEE Trans Syst Man, Cybern: Syst 2020;50(8):2978–88.

[25] Xue X, Fang J, Ai X, Cui S, Jiang Y, Yao W, Wen J. A fully distributed ADP algorithm for real-time economic dispatch of microgrid. IEEE Trans Smart Grid 2024;15(1):513–28.

[26] He Y, Wang W, Wu X. Multi-agent based fully distributed economic dispatch in microgrid using exact diffusion strategy. IEEE Access 2020;8:7020–31.

[27] Li Q, Gao DW, Zhang H, Wu Z, Wang F-y. Consensus-based distributed economic dispatch control method in power systems. IEEE Trans Smart Grid 2019;10(1):941–54.

[28] Lahmer A, Chang J-W, Park S, Jeong H, Chae S. Consensus-based adaptive distributed hierarchical control of battery energy storage systems in a DC microgrid. J Energy Storage 2024;97:112948.

[29] Simpson-Porco JW, Shafiee Q, Dorfler F, Vasquez JC, Guerrero JM, Bullo F. Secondary frequency and voltage control of islanded microgrids via distributed averaging. IEEE Trans Ind Electron 2015;62(11):7025–38.
[30] Han H, Li J, Wang H, Shi G, Xia Q, Sun Y, Liu Z. Distributed bus voltage regulation and economic dispatch for multi-bus AC microgrids. Int J Electr Power Energy Syst 2024;159:110017.
[31] Espina E, Cárdenas-Dobson RJ, Simpson-Porco JW, Kazerani M, Sáez D. A consensus-based distributed secondary control optimization strategy for hybrid microgrids. IEEE Trans Smart Grid 2023;14(6):4242–55.
[32] Dorfler F, Simpson-Porco JW, Bullo F. Breaking the hierarchy: distributed control and economic optimality in microgrids. IEEE Trans Control Netw Syst 2016;3(3):241–53.
[33] Jamali M, Baghaee HR, Sadabadi MS, Gharehpetian GB, Anvari-Moghaddam A. Distributed cooperative event-triggered control of cyber-physical AC microgrids subject to denial-of-service attacks. IEEE Trans Smart Grid 2023;14(6):4467–78.
[34] Yang C, Zheng T, Bu M, Li P, Guerrero JM. Distributed model-free adaptive control strategy for hybrid AC/DC Microgrid With Event-Triggered Mechanism. IEEE Trans Ind Electron 2024;71(8):9077–86.
[35] Zhang J, Sun B, Zhao D. A novel event-triggered secondary control strategy for distributed generalized droop control in microgrid considering time delay. IEEE Trans Power Electron 2023;38(5):5963–78.
[36] Zeng J, Liu T, Xu C, Sun Z. Distributed event-triggered current sharing consensus-based adaptive droop control of DC microgrid. Electronics 2025;14(6).
[37] Hu C, Zhang X, Wu Q. Accelerated dynamic event-triggered algorithm for online power system optimization by using powerball technique. IEEE Trans Smart Grid 2025;16(3):2348–60.
[38] Olfati-Saber R, Murray R. Consensus problems in networks of agents with switching topology and time-delays. IEEE Trans Autom Control 2004;49(9):1520–33.
[39] Hamad BR, Al-Durra A, Al-Jaafari KA, Zeineldin H, Mohamed YA-RI, El-Saadany E. Improving the robustness of distributed secondary control in autonomous microgrids to mitigate the effects of communication delays. Appl Energy 2024;364:123167.
[40] Jankovic N, Roldán-Pérez J, Prodanovic M, Rouco L. Centralised multimode power oscillation damping controller for photovoltaic plants with communication delay compensation. IEEE Trans Energy Convers 2024;39(1):311–21.
[41] Zhang C, Zhao J, Dou X, Hu Q, Leng J, Liu K. Containment-based distributed cooperative control of microgrid clusters: Accurately constraining the bus states of loads and microgrids. IEEE Trans Power Syst 2024;39(4):5741–54.
[42] Egido I, Fernandez-Bernal F, Rouco L. The Spanish AGC system: description and analysis. IEEE Trans Power Syst 2009;24(1):271–8.
[43] Chen G, Lewis FL, Feng EN, Song Y. Distributed optimal active power control of multiple generation systems. IEEE Trans Ind Electron 2015;62(11):7079–90.
[44] Wood AJ, Wollenberg BF, Sheblé GB. Power generation, operation, and control. John Wiley & Sons; 2013.
[45] Diestel R. Graph theory. New York: Springer; 2000, p. 415,
[46] Bidram A, Nasirian V, Davoudi A, Lewis FL. Cooperative synchronization in distributed microgrid control. In: Advances in industrial control, Cham, Switzerland: Springer International Publishing; 2017.
[47] Chu H, Yue D, Gao L, Lai X. Consensus of multiagent systems with relative state saturations. IEEE Trans Syst Man, Cybern: Syst 2021;51(4):2391–402.
[48] Chen G, Zhao Z. Delay effects on consensus-based distributed economic dispatch algorithm in microgrid. IEEE Trans Power Syst 2018;33(1):602–12.
[49] Tomás-Martín A, Zuluaga-Ríos CD, Suárez-Porras J, Kazemtabrizi B, García-Aguilar J, Sigrist L, García-Cerrada A. A vector-based flexible-complexity tool for simulation and small-signal analysis of hybrid AC/DC power systems. Sustain Energy, Grids Networks 2025;43:101817.
[50] Zimmerman RD, Murillo-Sánchez CE, Thomas RJ. MATPOWER: steady-state operations, planning, and analysis tools for power systems research and education. IEEE Trans Power Syst 2011;26(1):12–9.
[51] VFlexP. 2025, https://github.com/atomasmartin/VFlexP, GitHub repository.
[52] Johnson CR. Positive definite matrices. Am Math Mon 1970;77(3):259–64.